© APR 2026 | IRE Journals | Volume 9 Issue 10 | ISSN: 2456-8880
DOI: https://doi.org/10.64388/IREV9I10-1716693

Investigation Of Electromagnetohydrodynamic (EMHD) Fluid Flow Over an Exponentially Expanding Surface

OJO, ADETOYE SOLOMON[1], CHUKWUOCHA, IKECHUKWU JEREMIAH[2]
[1, 2]*Department of Physics, University of Port Harcourt, Choba, Nigeria*

Abstract- ***Electromagnetohydrodynamic (EMHD) flow over deforming surfaces has attracted considerable attention due to its importance in controlling transport phenomena in electrically conducting fluids. In this study, the characteristics of EMHD fluid flow and heat transfer over an exponentially expanding surface are investigated, accounting for the effects of thermal radiation and Joule heating. The governing nonlinear boundary layer equations, incorporating electromagnetic body forces, exponential surface expansion, and energy dissipation, are transformed into a solvable form and handled using the Fourier transform technique, which provides an efficient and accurate framework for analyzing the flow system. Thermal radiation is modeled using the Rosseland approximation to capture radiative heat flux within the fluid. Numerical evaluation of the transformed solutions is carried out to examine the influence of key dimensionless parameters on velocity and temperature distributions. The results indicate that an increase in the Prandtl number leads to a reduction in temperature profiles, reflecting enhanced thermal diffusion effects. Additionally, an increase in magnetic field strength suppresses the fluid velocity while thickening the thermal boundary layer, whereas higher radiation parameters elevate the temperature distribution within the flow domain. The exponential expansion parameter is also found to significantly influence both momentum and thermal fields. Overall, the study provides deeper insight into the behavior of EMHD flows over exponentially expanding surfaces and demonstrates the effectiveness of the Fourier transform approach in predicting heat transfer and flow characteristics in such systems.***

Index Terms- ***Electromagnetohydrodynamic (EMHD) flow, Fourier transform method, Heat transfer, Thermal radiation, Joule heating, exponentially expanding surface.***

I. INTRODUCTION

Modern industrial and engineering processes increasingly rely on precise control of transport phenomena in electrically conducting fluids subjected to coupled thermal and electromagnetic fields. Applications such as polymer extrusion, fiber drawing, continuous casting, thin-film coating, and semiconductor fabrication involve complex interactions between momentum and heat transfer within thin boundary layers formed over moving or deforming surfaces. The behavior of these boundary layers plays a critical role in determining product quality, including surface uniformity, microstructural integrity, and mechanical performance. Inadequate control of these processes often leads to defects, thermal stresses, and non-uniform cooling, thereby reducing material efficiency and reliability (Fatunmbi and Are, 2025; Muhammad et al., 2023).

The study of magnetohydrodynamics (MHD) has provided significant insight into the manipulation of electrically conducting fluids through magnetic fields. The induced Lorentz force alters fluid motion and energy transport without direct mechanical interaction. Building on this framework, electromagnetohydrodynamics (EMHD) extends the concept by incorporating both electric and magnetic fields, offering enhanced flexibility in controlling fluid flow, heat transfer, and mass transport. This approach is particularly relevant in microscale systems, high-temperature environments, and precision manufacturing processes where conventional control mechanisms are limited (Muzara and Shateyi, 2023; Kayalvizhi and Vijayakumar, 2022).

Recent studies have explored the behavior of nanofluids and conducting fluids under MHD and EMHD effects. For instance, investigations into MHD silver nanofluid flow over cylindrical geometries have demonstrated the significant influence of material properties and electromagnetic parameters on velocity, temperature, and concentration profiles. These studies employed analytical techniques such as the Laplace transform and incorporated thermal conductivity and viscosity

© APR 2026 | IRE Journals | Volume 9 Issue 10 | ISSN: 2456-8880
DOI: https://doi.org/10.64388/IREV9I10-1716693

models to describe transport behavior. The results highlighted the role of magnetic fields in modifying boundary layer thickness and enhancing or suppressing heat transfer characteristics, depending on the governing parameters (Adetoye et al., 2025; Ojo et al., 2025).

Further analyses have emphasized the importance of key dimensionless parameters, including the Prandtl number, radiation parameter, and magnetic field strength, in determining thermal and flow characteristics. It has been consistently observed that increasing the Prandtl number reduces thermal boundary layer thickness, while radiation effects tend to elevate temperature distributions. These findings establish a strong foundation for extending MHD studies to more advanced EMHD configurations, where additional control can be achieved through electric field interactions.

In many industrial applications, surface-driven flows arise due to stretching or expansion of substrates, leading to nonlinear velocity distributions and complex thermal boundary layers. Exponentially expanding surfaces, in particular, are relevant in processes involving rapid stretching rates and non-uniform deformation. The presence of thermal radiation becomes increasingly important at elevated temperatures, contributing significantly to the overall heat transfer mechanism. Additionally, Joule heating, resulting from electrical current dissipation, can influence thermal energy distribution within the fluid, either enhancing heat transfer or causing undesirable localized overheating if not properly controlled (Albuquerque et al., 2024; Sulochana, 2024).

Modeling EMHD flows over such surfaces presents substantial mathematical challenges due to the nonlinear coupling between momentum, energy, and electromagnetic equations. Various numerical and analytical techniques have been proposed to address these complexities. In particular, Fourier-based methods have gained attention for their high accuracy, fast convergence, and efficiency in solving boundary layer problems with complex geometries and parameter dependencies. Studies employing Fourier spectral approaches have demonstrated improved numerical stability and solution accuracy when analyzing EMHD flows with radiation and Joule heating effects (Ramesh, 2022; Abdelmalek, 2023).

Motivated by these developments, the present study investigates EMHD fluid flow and heat transfer over an exponentially expanding surface using a Fourier transform framework. The analysis incorporates the combined effects of electromagnetic forcing, thermal radiation, and Joule heating on boundary layer behavior. By examining the influence of key governing parameters on velocity and temperature distributions, this work aims to provide deeper insight into EMHD transport mechanisms and contribute to the advancement of efficient flow and thermal control strategies in engineering applications.

II. MATHEMATICAL FORMULATION OF THE PROBLEM

The fundamental partial differential equations governing the effects of chemical reactions and thermal radiation are the continuity, momentum, energy, and concentration equations.

$$\frac{\partial v_r}{\partial r}+\frac{\partial \rho}{\partial t}=0 \tag{1}$$

$$\rho\frac{\partial u_{(r)}}{\partial t}+\nabla\rho-\mu\nabla^2 u=g\beta_\theta\left(\theta-\theta_*\right)+g\beta_\phi\left(\phi-\phi_*\right)-\left(\sigma B_0^2 u_r+\sigma_0\right) \tag{2}$$

$$\left(\rho C_p\right)\frac{\partial \theta_{(r)}}{\partial r}+\frac{\partial}{\partial r}\left(q_{(r)}\right)=K\frac{\partial^2\theta}{\partial r^2} \tag{3}$$

$$\left(\rho C_p\right)\frac{\partial \phi}{\partial r}+K_0^2\phi=D\frac{\partial^2\phi}{\partial r^2} \tag{4}$$

For an incompressible EMHD fluid under steady-state conditions in a Cartesian coordinate system, equation (2) - (4), together with equation (1), are transformed into

$$\frac{1}{\rho}\mu\nabla^2 u-\frac{1}{\rho}\nabla\rho+\frac{g\beta_\theta\left(\theta-\theta_*\right)}{\rho}+\frac{g\beta_\phi\left(\phi-\phi_*\right)}{\rho}-\frac{\sigma B_0^2 u_r}{\rho}-\frac{\sigma_0}{u_r}=0 \tag{5}$$

$$\frac{1}{\left(\rho C_p\right)}K\frac{\partial^2\theta}{\partial r^2}-\frac{1}{\left(\rho C_p\right)}\frac{\partial}{\partial r}\left(q_{(r)}\right)=0 \tag{6}$$

$$\frac{1}{\left(\rho C_p\right)}D\frac{\partial^2\phi}{\partial r^2}-\frac{1}{\left(\rho C_p\right)}K_0^2\phi=0 \tag{7}$$

© APR 2026 | IRE Journals | Volume 9 Issue 10 | ISSN: 2456-8880
DOI: https://doi.org/10.64388/IREV9I10-1716693

Where u is fluid velocity, $\theta$is temperature, ρ is fluid density, μ is viscosity of fluid, C_p is specific heat at persistent pressure, q_r is radiation term, K is thermal conductivity of fluid, K_0 is chemical reaction term, D is chemical molecular diffusivity, ϕ is fluid concentration.

By using Rosseland approximation (q_y) to consider the effect of radiation on an optically thick model in which the thermal layer becomes very thick.

$$q_{(r)} = -\frac{1}{3\alpha} 4K_B \frac{\partial}{\partial r}\theta^4 \quad (8)$$

Where K_B is the Stefan-Boltzmann constant and α denotes the absorption coefficient. It is presumed that the temperature variation in the flow is minimal enough for θ^4 can be expressed as a linear function of temperature. This is accomplished by expanding θ^4 in a Taylor series about θ_∞ and neglect higher order terms, the expression results in to

$$\theta^4 = 4\theta_\infty^3\theta - 3\theta_\infty^4 \quad (9)$$

Using equation (8) and (9), equation (6) takes the form

$$\frac{\rho}{r}\frac{\partial\theta}{\partial r} = \frac{1}{\left(\rho\hat{C}_p\right)}K\left(1+\frac{16K_0\theta^3}{3\alpha}\right)\frac{1}{r}\frac{\partial}{\partial r}\left(r\frac{\partial\theta}{\partial r}\right) - \frac{1}{\left(\rho\hat{C}_p\right)}K\frac{1}{r}q_{(r)} \quad (10)$$

III. DIMENSIONAL ANALYSIS

Equations (5) - (7) are non-dimensionalized using the Schmidt number, Prandtl number, Grashof number, radiation parameter, heat generation parameter, electrical conductivity parameter, and magnetic field parameter. The corresponding dimensionless variables are given as:

$$\mathrm{Pr} = \frac{k(\rho Cp)}{k\left(\rho C_p\right)}, Sc = \frac{k\left(\rho C_p\right)}{D\left(\rho C_p\right)}, \mathrm{Re}^{-1} = \frac{\mu\rho}{\rho\mu}, u = \frac{v_r t^*}{r}, r = \frac{r^*}{d}, k_0 = \frac{k_r^2\left(\rho C_p\right)}{\left(\rho C_p\right)v^{*2}},$$

$$\theta = \frac{T-T_0}{T_0}, C = \frac{C-C_0}{C_0}, \Re = \frac{16\zeta\theta_0^3\rho}{3\alpha\left(C_p\right)}, H_a = \frac{\sigma B_0^2 v_r}{\rho}, \sigma_0 = \frac{\sigma_0}{v_r},$$

$$Gr_\theta = \frac{g\beta(T-T_0)\mu}{v_r^2\beta}, Gr_c = \frac{g\beta^*(C-C_0)\mu}{v_r^2\beta^*},$$

Rewriting equations (5), (7) and (10) in dimensionless form, the modelled equations are transformed into

$$\mathrm{Re}^{-1}\left(\frac{1}{r}\frac{\partial v_r}{\partial r}+\frac{\partial^2 v_r}{\partial r^2}\right) - \frac{1}{r}\frac{\partial v_r}{\partial r} + Gr_\theta\theta + Gr_\phi\phi - \left(H_a v_r + \sigma_0 v_r\right) = 0 \quad (11)$$

$$\mathrm{Pr}^{-1}\left(\frac{1}{r}\frac{\partial\theta}{\partial r}+\frac{\partial^2\theta}{\partial r^2}\right) - \frac{1}{r}\frac{\partial\theta}{\partial y} - \Re\left(\frac{1}{r}\frac{\partial\theta}{\partial r}+\frac{\partial^2\theta}{\partial r^2}\right) = 0 \quad (12)$$

$$Sc^{-1}\left(\frac{1}{r}\frac{\partial\phi}{\partial r}+\frac{\partial^2\phi}{\partial r^2}\right) - \frac{1}{r}\frac{\partial\phi}{\partial r} - \frac{1}{r}K_0 C = 0 \quad (13)$$

Where Re is Reynolds number, Pr is Prandlt number, Sc is Schmidt number, $G_{r_\theta}\theta$ is thermal Grashofs number, $G_{r_\phi}\phi$ is modified Grashofs number, $\Re$ is dimensionless radiation term, θ is dimensionless temperature, u is dimensionless velocity, ϕ is dimensionless concentration, H_a is magnetic Hartmann number, σ_0 is electroconductivity term k_0 is dimensionless chemical reaction term and r is dimensionless area of fluid flow.

IV. SOLUTION TECHNIQUE

Applying Fourier Transform Method to solve equation 11 – 13 then equation 13 can be

$$f(\omega)_{(C)} = \frac{1}{\sqrt{2\pi}\left(\left(\omega_0-\omega\right)-\frac{1}{2\tau}\right)}\left[\sin\left[\left(\omega_0-\omega\right)-\frac{1}{2\tau}\right]\left[\frac{1}{Sc}\frac{\partial^2\phi}{\partial r^2}+k_0\phi\right]\right] \quad (14)$$

If equation (14) experienced the constant Fourier Spectrum model then equation (14) becomes

$$\sqrt{2\pi}\left(\left(\omega_0-\omega\right)-\frac{1}{2\tau}\right) = \sin\left[\left(\omega_0-\omega\right)-\frac{1}{2\tau}\right]\left[Sc^{-1}\frac{\partial^2\phi}{\partial r^2}+k_0\phi\right] \quad (15)$$

$$Sc^{-1}\frac{\partial^2\phi}{\partial r^2}+k_0\phi=\frac{1}{\sin\left[\left(\omega_0-\omega\right)-\frac{1}{2\tau}\right]}\left[\sqrt{2\pi}\left(\left(\omega_0-\omega\right)-\frac{1}{2\tau}\right)\right] \quad (16)$$

$$\frac{\partial^2\phi}{\partial r^2}=-k_0\phi+Sc\left[\frac{\sqrt{2\pi}\left(\left(\omega_0-\omega\right)-\frac{1}{2\tau}\right)}{\sin\left[\left(\omega_0-\omega\right)-\frac{1}{2\tau}\right]}\right] \quad (17)$$

$$\iint\phi_{(r)}{}^{II}=\iint\left(-k_0\phi+Sc\left[\frac{\sqrt{2\pi}\left(\left(\omega_0-\omega\right)-\frac{1}{2\tau}\right)}{\sin\left[\left(\omega_0-\omega\right)-\frac{1}{2\tau}\right]}\right]\right) \quad (18)$$

Integrating equation (17) twice, equation (18) becomes

$$\phi_{(r)}=-\frac{1}{2}.\frac{1}{3}k_0r^3+Sc\left[\frac{\sqrt{2\pi}\left(\left(\omega_0-\omega\right)-\frac{1}{2\tau}\right)}{\sin\left[\left(\omega_0-\omega\right)-\frac{1}{2\tau}\right]}\right] \quad (19)$$

Fourier transform of equation (12) implies

$$f(\omega)_{(T)}=\frac{1}{\sqrt{2\pi}\left(\left(\omega_0-\omega\right)-\frac{1}{2\tau}\right)}\left[\sin\left[\left(\omega_0-\omega\right)-\frac{1}{2\tau}\right]\left[\Pr^{-1}\frac{\partial^2\theta}{\partial r^2}+\Re\theta\right]\right] \quad (20)$$

If equation (20) experienced the constant Fourier Spectrum model then equation (20) becomes

$$\sin\left[\left(\omega_0-\omega\right)-\frac{1}{2\tau}\right]\left[\Pr^{-1}\frac{\partial^2\theta}{\partial r^2}+\Re\theta\right]=\sqrt{2\pi}\left(\left(\omega_0-\omega\right)-\frac{1}{2\tau}\right) \quad (21)$$

$$\frac{1}{\Pr}\frac{\partial^2\theta}{\partial r^2}+\Re\theta=\frac{\sqrt{2\pi}\left(\left(\omega_0-\omega\right)-\frac{1}{2\tau}\right)}{\sin\left[\left(\omega_0-\omega\right)-\frac{1}{2\tau}\right]} \quad (22)$$

$$\frac{\partial^2\theta}{\partial r^2}=\Re\theta+\Pr\left[\frac{\sqrt{2\pi}\left(\left(\omega_0-\omega\right)-\frac{1}{2\tau}\right)}{\sin\left[\left(\omega_0-\omega\right)-\frac{1}{2\tau}\right]}\right] \quad (23)$$

$$\iint\theta_{(r)}^{II}=\iint\left(\Re\theta+\Pr\left[\frac{\sqrt{2\pi}\left(\left(\omega_0-\omega\right)-\frac{1}{2\tau}\right)}{\sin\left[\left(\omega_0-\omega\right)-\frac{1}{2\tau}\right]}\right]\right) \quad (24)$$

Integrating equation (23) twice, equation (24) results

$$\theta_{(r)}=\frac{1}{2}.\frac{1}{3}\Re r^3+\Pr\left[\frac{\sqrt{2\pi}\left(\left(\omega_0-\omega\right)-\frac{1}{2\tau}\right)}{\sin\left[\left(\omega_0-\omega\right)-\frac{1}{2\tau}\right]}\right] \quad (25)$$

Fourier transform of equation (11) implies

$$F(t)_{u_r}=\begin{cases}\left(\mathrm{Re}^{-1}\left(\frac{1}{r}\frac{\partial u_r}{\partial r}+\frac{\partial^2u_r}{\partial r^2}\right)-\frac{1}{r}\frac{\partial u_r}{\partial r}+Gr_\theta\theta+Gr_\phi\phi-\left(H_au_r+\sigma_0u_r\right)\right)e^{-\frac{t}{2\tau}}e^{i\omega_0t}\\ 0\end{cases} \quad (26)$$

Appling boundary conditions

$$\begin{matrix}t>0\\ t<0\end{matrix} \quad (27)$$

Equation (26) becomes

$$F(\omega)_{u_r}=\frac{1}{\sqrt{2\pi}}\int_{-1}^{1}\left(\frac{1}{\mathrm{Re}}\left[\frac{1}{r}\frac{\partial u_r}{\partial r}+\frac{\partial^2u_r}{\partial r^2}\right]-\frac{1}{r}\frac{\partial u_r}{\partial r}+Gr_\theta\theta+Gr_\phi\phi-H_au_r-\sigma_0u_r\right)e^{-\frac{t}{2\tau}}e^{i\omega_0t}e^{-i\omega t}dt \quad (28)$$

$$F(\omega)_{u_r}=\frac{\frac{1}{\mathrm{Re}}\left[\frac{1}{r}\frac{\partial u_r}{\partial r}+\frac{\partial^2u_r}{\partial r^2}\right]-\frac{1}{r}\frac{\partial u_r}{\partial r}+Gr_\theta\theta+Gr_\phi\phi-H_au_r-\sigma_0u_r}{\sqrt{2\pi}}\left[\frac{e^{i\left[\left(\omega_0-\omega\right)-\frac{1}{2\tau}\right]t}}{i\left[\left(\omega_0-\omega\right)-\frac{1}{2\tau}\right]}\right]_{-1}^{1} \quad (29)$$

© APR 2026 | IRE Journals | Volume 9 Issue 10 | ISSN: 2456-8880
DOI: https://doi.org/10.64388/IREV9I10-1716693

$$F(\omega)_{u_r}=\frac{\frac{1}{\mathrm{Re}}\left[\frac{1}{r}\frac{\partial u_r}{\partial r}+\frac{\partial^2 u_r}{\partial r^2}\right]-\frac{1}{r}\frac{\partial u_r}{\partial r}+Gr_\theta\theta+Gr_\phi\phi-H_a u_r-\sigma_0 u_r}{\sqrt{2\pi}}\left[\frac{e^{i\left[(\omega_0-\omega)-\frac{1}{2\tau}\right](1)}-e^{-i\left[(\omega_0-\omega)-\frac{1}{2\tau}\right](-1)}}{i\left[(\omega_0-\omega)-\frac{1}{2\tau}\right]}\right] \quad (30)$$

$$F(\omega)_{u_r}=\frac{\frac{1}{\mathrm{Re}}\left[\frac{1}{r}\frac{\partial u_r}{\partial r}+\frac{\partial^2 u_r}{\partial r^2}\right]-\frac{1}{r}\frac{\partial u_r}{\partial r}+Gr_\theta\theta+Gr_\phi\phi-H_a u_r-\sigma_0 u_r}{\sqrt{2\pi}}\left[\frac{e^{i\left[(\omega_0-\omega)-\frac{1}{2\tau}\right]}-e^{-i\left[(\omega_0-\omega)-\frac{1}{2\tau}\right]}}{i\left[(\omega_0-\omega)-\frac{1}{2\tau}\right]}\right] \quad (31)$$

Appling Euler's Identity

$$e^{i\phi}=Cos\phi+iSin\phi \quad (32)$$

$$e^{i\left[(\omega_0-\omega)-\frac{1}{2\tau}\right]}=Cos\left[(\omega_o-\omega)-\frac{1}{2\tau}\right]+iSin\left[(\omega_o-\omega)-\frac{1}{2\tau}\right] \quad (33)$$

Also $$e^{-i\phi}=Cos\phi-iSin\phi \quad (34)$$

$$e^{-i\left[(\omega_0-\omega)-\frac{1}{2\tau}\right]}=Cos\left[(\omega_o-\omega)-\frac{1}{2\tau}\right]-iSin\left[(\omega_o-\omega)-\frac{1}{2\tau}\right] \quad (35)$$

Substituting equation (33) and (35) into equation (31) it gives

$$F(\omega)_{u_r}=\frac{\frac{1}{\mathrm{Re}}\left[\frac{1}{r}\frac{\partial u_r}{\partial r}+\frac{\partial^2 u_r}{\partial r^2}\right]-\frac{1}{r}\frac{\partial u_r}{\partial r}+Gr_\theta\theta+Gr_\phi\phi-H_a u_r-\sigma_0 u_r}{\sqrt{2\pi}}\left[\frac{\left(Cos\left[(\omega_o-\omega)-\frac{1}{2\tau}\right]+iSin\left[(\omega_o-\omega)-\frac{1}{2\tau}\right]\right)-\left(Cos\left[(\omega_o-\omega)-\frac{1}{2\tau}\right]-iSin\left[(\omega_o-\omega)-\frac{1}{2\tau}\right]\right)}{i\left[(\omega_0-\omega)-\frac{1}{2\tau}\right]}\right] \quad (36)$$

$$F(\omega)_{u_r}=\frac{\frac{1}{\mathrm{Re}}\left[\frac{1}{r}\frac{\partial u_r}{\partial r}+\frac{\partial^2 u_r}{\partial r^2}\right]-\frac{1}{r}\frac{\partial u_r}{\partial r}+Gr_\theta\theta+Gr_\phi\phi-H_a u_r-\sigma_0 u_r}{\sqrt{2\pi}}\left[\frac{Sin\left[(\omega_o-\omega)-\frac{1}{2\tau}\right]}{i\left[(\omega_0-\omega)-\frac{1}{2\tau}\right]}\right] \quad (37)$$

If equation (37) experienced the constant Fourier Spectrum model and then integrated twice thus, equation (37) implies (38)

$$\iint u^{II}_{(r)}=\mathrm{Re}\left[-Gr_\phi\phi-Gr_\theta\right]-\frac{1}{2}.\frac{1}{3}\left[H_a-\sigma_0\right]r^3 \quad (38)$$

Substitute equation (19) and (25) into equation (38) it becomes

$$u_{(r)}=\mathrm{Re}\left[-Gr_\phi\left[-\frac{1}{2}.\frac{1}{3}.k_0 r^3+Sc\left(\frac{\sqrt{2\pi}\left(\omega_0-\omega\right)-\frac{1}{2\tau}}{Sin\left[\left(\omega_0-\omega\right)-\frac{1}{2\tau}\right]}\right)\right]-Gr_\theta\left[-\frac{1}{2}.\frac{1}{3}.\Re r^3+\mathrm{Pr}\left(\frac{\sqrt{2\pi}\left(\omega_0-\omega\right)-\frac{1}{2\tau}}{Sin\left[\left(\omega_0-\omega\right)-\frac{1}{2\tau}\right]}\right)\right]-\frac{1}{2}.\frac{1}{3}.\left[H_a-\sigma_0\right]r^3 \quad (39)$$

Table 1: Selected realistic values of dimensionless hydrodynamic parameters

Parameters	Value
Prandtl number (*Pr*)	3.5, 7.0, 10.5, 14.0, 17.5
Reynolds number (*Re*)	10, 20, 30, 40, 50
Schmidt number (*Sc*)	2.5, 4.5, 6.5, 8.5, 10.5
Radiation term ($\Re$)	3.5, 6.5, 9.5, 12.5, 15.5
Grashof number (Gr_ϕ) due to concentration	3.2, 6.4, 9.6, 12.8, 16.0
Grashof number (Gr_θ) due to temperature	2.6, 5.2, 7.8, 10.4, 13.0
Magnetic Hartmann Number (Ha)	0.5, 1.5, 2.5, 3.5, 4.5
Chemical reaction term (k_0)	1.8, 3.6, 5.4, 7.2, 9.0
Electro-conductivity term (σ_0)	0.25, 0.50, 1.75, 1.00, 1.25

V. RESULTS AND DISCUSSION

To gain deeper physical insight into the electromagnetohydrodynamic (EMHD) flow problem and its relevance to advanced material processing, Eqs. (19), (25), and (39), together with the modified

boundary conditions in Eq. (27), are solved numerically using the Fourier transform method. The corresponding computational fluid dynamics results over an exponentially stretching surface are presented in Table 1 and illustrated graphically in Figures 1–16.

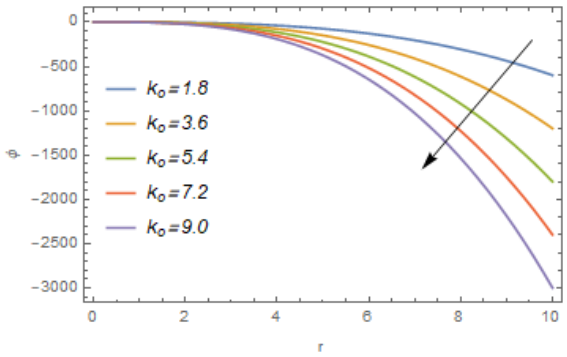

Figure 1. Concentration profile ϕ in relation to boundary layer r for different values of chemical reaction term k_0.

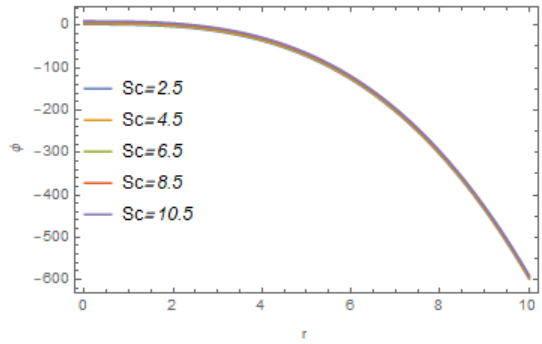

Figure 2. Concentration profile ϕ in relation to boundary layer r for different values of Schmidt number Sc.

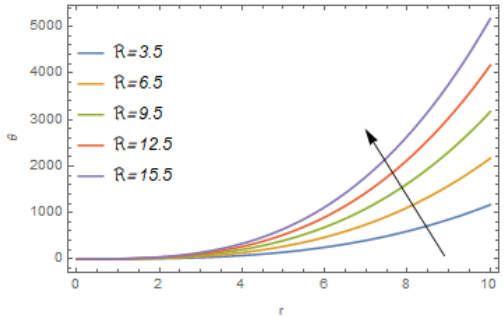

Figure 3. Temperature profile θ in relation to boundary layer r for different values of Radiation term $(\Re)$.

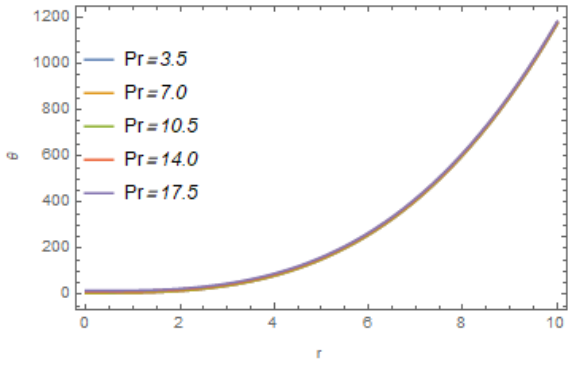

Figure 4. Temperature profile θ in relation to boundary layer r for different values of Prandtl number Pr

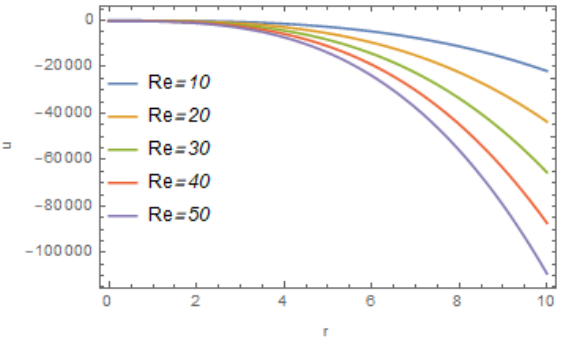

Figure 5. Velocity profile u in relation to boundary layer r for different values of Reynolds number (Re).

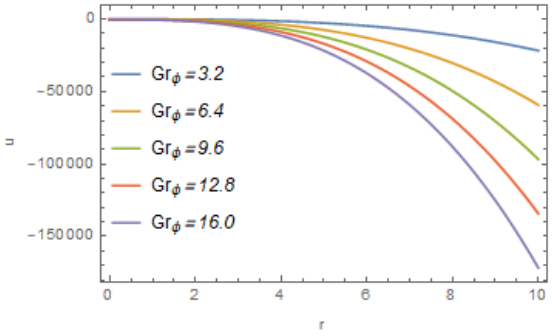

Figure 6. Velocity profile u in relation to boundary layer r for different values of Grashof number in term of concentration (Gr_ϕ).

© APR 2026 | IRE Journals | Volume 9 Issue 10 | ISSN: 2456-8880
DOI: https://doi.org/10.64388/IREV9I10-1716693

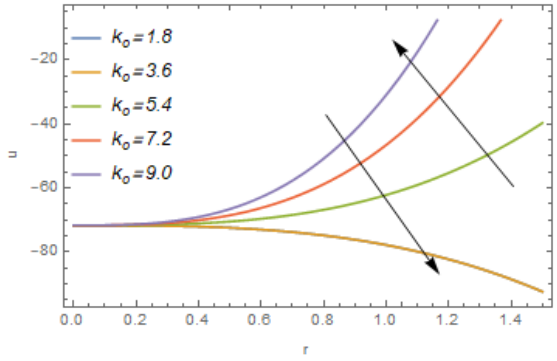

Figure 7. Velocity profile u in relation to boundary layer r for different values of chemical reaction term (k_0).

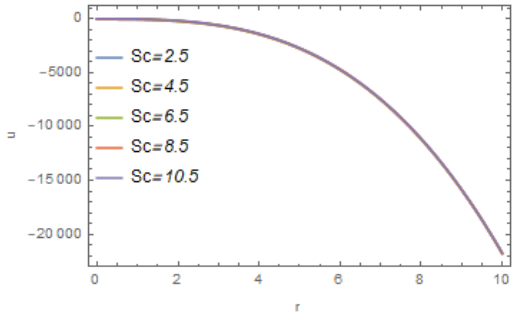

Figure 8. Velocity profile u in relation to boundary layer r for different values of Schmidt number (Sc)

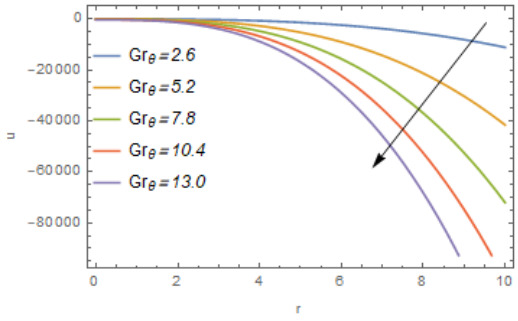

Figure 9. Velocity profile u in relation to boundary layer r for different values of Grashof number in term of temperature (Gr_θ).

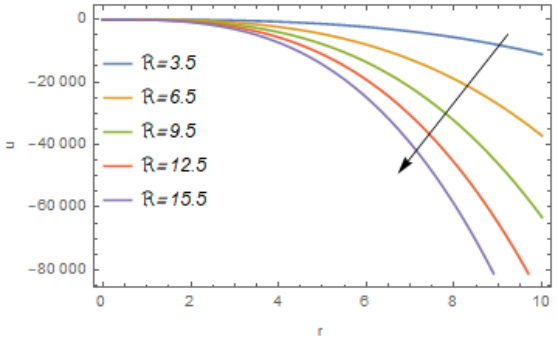

Figure 10. Velocity profile u in relation to boundary layer r for different values of Radiation term $(\Re)$.

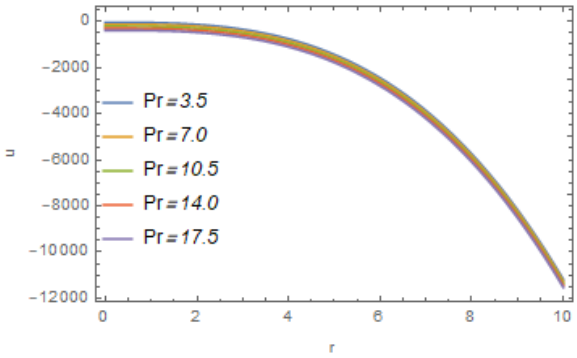

Figure 11. Velocity profile u in relation to boundary layer r for different values of Prandtl number (Pr).

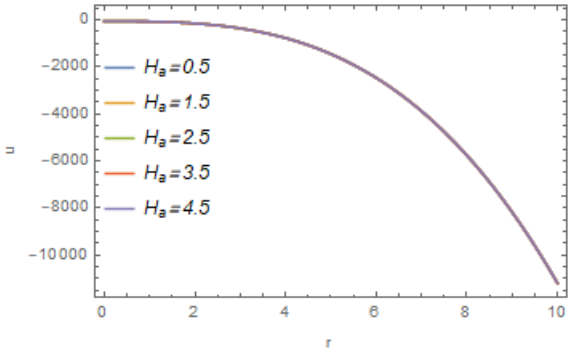

Figure 12. Velocity profile u in relation to boundary layer r for different values of Magnetic Hartmann number (H_a).

© APR 2026 | IRE Journals | Volume 9 Issue 10 | ISSN: 2456-8880
DOI: https://doi.org/10.64388/IREV9I10-1716693

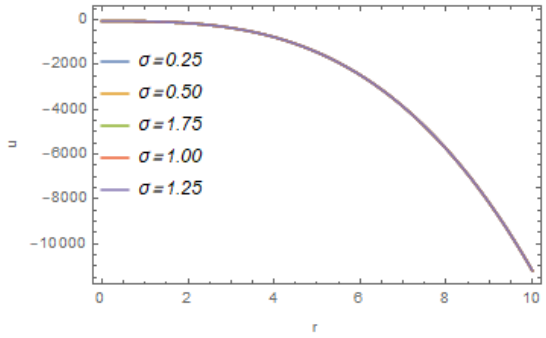

Figure 13. The velocity profile u in relation to the boundary layer r for different values of the Electroconductivity parameter (σ).

Figure 1: illustrates the variation of the concentration profile within the boundary layer for different values of the chemical reaction parameter. It is observed that increasing the chemical reaction parameter significantly reduces species concentration throughout the flow domain. Physically, stronger chemical reactions accelerate the consumption of diffusing species, leading to lower concentration levels near the surface and in the free stream. This reduction enhances control over mass transport processes and improves reaction efficiency. Such behavior is particularly useful in applications like catalytic surface reactions, chemical vapor deposition, and corrosion control. The results are consistent with Solomon et al. (2025).

Figure 2: presents the concentration distribution for varying values of the Schmidt number. An increase in the Schmidt number reduces mass diffusivity relative to momentum diffusivity, resulting in a thinner concentration boundary layer. This indicates slower species diffusion from the surface into the fluid. The effect is crucial in processes where controlled diffusion is required, such as drying technologies, polymer blending, and gas absorption systems. Proper tuning of this parameter ensures uniform material properties and efficient transport processes.

Figure 3: depicts the temperature distribution for different thermal radiation parameters. The results show that increasing the radiation parameter elevates the temperature within the boundary layer due to enhanced radiative heat flux. This demonstrates the strong influence of radiation on thermal transport, especially at high operating temperatures. Such effects are important in thermal coating, furnace design, and high-temperature manufacturing systems. The findings also highlight the need to carefully regulate radiative heat transfer to prevent overheating and maintain material integrity.

Figure 4: shows the influence of the Prandtl number on temperature distribution. As the Prandtl number increases, the thermal boundary layer thickness decreases, indicating improved heat transfer rates. This occurs because higher Prandtl numbers correspond to lower thermal diffusivity. The result is significant in cooling systems, heat exchangers, and polymer processing, where efficient heat removal is required. Controlling this parameter helps achieve better thermal regulation and improved product quality.

Figure 5 illustrates the velocity profile for varying Reynolds number values. The results indicate that increasing the Reynolds number enhances momentum transport, leading to higher flow velocity along the surface. This reflects the dominance of inertial forces over viscous forces in the flow system. Such behavior is beneficial in processes requiring rapid fluid motion, including extrusion, coating flows, and fluid transport systems. However, excessive Reynolds numbers may lead to flow instability, which must be carefully managed.

Figure 6: presents the effect of the solutal Grashof number on velocity distribution. It is observed that velocity increases with higher values of the solutal Grashof number due to enhanced buoyancy forces arising from concentration gradients. This indicates that concentration-driven convection plays a significant role in momentum transport. The effect is particularly relevant in natural convection systems, chemical reactors, and environmental flow processes. It can also be utilized to improve mixing and enhance mass transfer efficiency.

Figure 7 demonstrates the influence of the chemical reaction parameter on the velocity profile. The results reveal that chemical reactions significantly affect momentum transport by interacting with diffusion and buoyancy mechanisms. Stronger reactions modify the flow structure and can either enhance or

suppress fluid motion depending on system conditions. This is important in reactive flow systems such as combustion, catalytic processing, and chemical synthesis. It provides a pathway for controlling flow behavior in reactive manufacturing environments.

Figure 8: shows the effect of the Schmidt number on velocity distribution, emphasizing the coupling between mass diffusion and momentum transport. As the Schmidt number increases, changes in diffusivity alter the velocity field within the boundary layer. This interaction is critical in processes involving simultaneous heat and mass transfer, such as coating technologies and separation processes. Proper control ensures uniform deposition and improved efficiency in material fabrication systems.

Figure 9: illustrates the velocity variation with the thermal Grashof number. The results indicate that velocity increases with higher thermal Grashof numbers due to stronger thermal buoyancy forces. This enhances convective motion and improves heat transfer within the boundary layer. The effect is particularly useful in natural convection cooling systems, solar energy devices, and thermal management applications. It also contributes to improved temperature uniformity in industrial processes.

Figure 10: presents the influence of thermal radiation on the velocity field. The results show that radiative heat transfer significantly modifies momentum transport, demonstrating the strong coupling between thermal and flow characteristics. Increased radiation leads to higher energy levels within the fluid, which in turn affects velocity distribution. This is important in high-temperature environments such as furnaces, combustion chambers, and thermal reactors. Controlling radiation effects can improve efficiency and prevent thermal damage.

Figure 11: shows the effect of the Prandtl number on velocity distribution, confirming that thermal diffusivity influences momentum transport. Variations in this parameter alter the interaction between thermal and velocity boundary layers. This is particularly relevant in heat transfer equipment and fluid processing systems. Proper adjustment of the Prandtl number ensures optimal coupling between heat and momentum transport, enhancing system performance.

Figure 12: illustrates the influence of the Hartmann number on velocity profiles. Increasing the Hartmann number strengthens electromagnetic (Lorentz) forces, which suppress fluid motion and stabilize the flow. This effect is crucial in EMHD systems where magnetic fields are used for flow control. Applications include electromagnetic pumps, metallurgical processes, and cooling of nuclear reactors. The results agree with Adetoye et al. (2025).

Figure 13: presents the variation of velocity with the electrical conductivity parameter. The results confirm that electrical conductivity significantly influences EMHD flow behavior by enhancing electromagnetic interactions. Higher conductivity improves the responsiveness of the fluid to applied fields, allowing better control of momentum transport. This is highly relevant in microfluidics, coating technologies, and advanced manufacturing systems. The findings align with Ojo et al. (2025).

CONCLUSION

This study has examined electromagnetohydrodynamic (EMHD) fluid flow and heat transfer over an exponentially expanding surface using the Fourier transform method. The analysis highlights the combined influence of electromagnetic effects, thermal radiation, Joule heating, and key dimensionless parameters on the boundary layer characteristics. It is observed that magnetic effects play a dominant role in regulating fluid motion through Lorentz forces, while also influencing thermal behavior within the flow domain. The Fourier-based approach proves to be efficient and accurate in handling the coupled nonlinear governing equations. Overall, the results provide a clear understanding of how EMHD parameters can be manipulated to control momentum and heat transfer processes in technologically relevant systems.

1. The Fourier transform method provides an accurate and computationally efficient framework for solving EMHD flow over an exponentially expanding surface.

2. Magnetic field strength significantly suppresses velocity profiles due to Lorentz force effects, thereby enhancing flow control.
3. Thermal radiation and Joule heating contribute to increased temperature distribution and thicker thermal boundary layers.
4. Dimensionless parameters such as Reynolds, Prandtl, Schmidt, and Grashof numbers strongly govern the interaction between momentum and heat transfer.
5. EMHD parameters can be effectively tuned to optimize heat and mass transfer processes in applications such as coating, extrusion, and thermal management systems.

REFERENCES

[1] A.S. Ojo, A. T. Ngiangia, M. C. Onyeaju. (2025). Comparative effects of energy transfer on silver nanofluid in magnetohydrodynamic flow via the cylindrical surface". *Journal of Nanofluids*. Vol. 14, pp, 1-11.

[2] A.S. Ojo, A. T. Ngiangia, M. C. Onyeaju. (2025). Numerical analysis of energy transfer on magnetohydrodynamic silver nanofluid flow in cylindrical coordinate. *Open Journal of Physical Science*. Vol 6, pp, 63-82.

[3] Abdelmalek, Z., & Saeed, T. (2023). Fourier spectral collocation simulation of EMHD boundary-layer flow over stretching surfaces. *Computers & Mathematics with Applications*, 136, 45–60.

[4] Adetoye S, O., Alalibo, N., Onyeaju M., and Chijioke A, E. (2025). Energy transfer on magnetohydrodynamic silver nanofluid flow past a cylindrical enclosure. *Journal of Nanofluid*, Vol. 14, pp. 639-648.

[5] Albuquerque, L. A. V. d., Villela, M. F. d. S., & Mariano, F. P. (2024). Numerical simulation of flows using the Fourier pseudospectral method and the immersed boundary method. *Axioms*, 13(4), 228. https://doi.org/10.3390/axioms13040228

[6] Fatunmbi, E. O., & Are, S. O. (2025). Numerical investigation of MHD nanofluid

[7] flow over an exponentially stretching porous sheet with activation energy and non-uniform heat source. *Journal of Engineering Research and Reports*, 27(6), 214–223. https://doi.org/10.9734/jerr/2025/v27i61539.

[8] Kayalvizhi, J., & Vijaya Kumar, A. G. (2022). Entropy analysis of EMHD hybrid nanofluid stagnation point flow over a porous stretching sheet with thermal radiation. *Energies*, 15(21), 8317. https://doi.org/10.3390/en15218317

[9] Muhammad, K., Ahmed, B., Sharaf, M., Afikuzzaman, M., & Az-Zo'bi, E. A. (2023).

[10] Multiscale tribology analysis of MHD hybrid nanofluid flow over a curved stretching surface. *Nanoscale Advances*, 6, 855–866. https://doi.org/10.1039/D3NA00723A

[11] Muzara, H., & Shateyi, S. (2023). Magnetohydrodynamics Williamson nanofluid flow over an exponentially stretching surface with chemical reaction and thermal radiation. *Mathematics*, 11(12), 2740. https://doi.org/10.3390/math11122740.

[12] Nascimento, A. A., da Silveira Neto, A., & Mariano, F. P. (2024). Coupling of the immersed boundary and Fourier pseudo-spectral methods applied to fluid–structure interaction problems. *Journal of the Brazilian Society of Mechanical Sciences and Engineering*, 46, 213. https://doi.org/10.1007/s40430-024-03600-5

[13] Nikodijević Đorđević, M. D., Petrović, J. D., Kocić, M. M., Stamenković, Ž. M., & Nikodijević, D. D. (2025). EMHD flow and heat transfer of a nanofluid layer and a hybrid nanofluid layer in a horizontal channel with porous medium. *Applied Sciences*, 15(18), 10183. https://doi.org/10.3390/app151810183

[14] Ojo, A. S., & Egbo, C. A. (2025) Effect of radiation and chemical reaction on ozone layer healing. *Open Journal of Physical Science,* Vol. 6 (2), Pg: 01 – 13.

[15] Ramesh, G. K., Roopa, G. S., & Prasannakumara, B. C. (2022). EMHD flow and heat transfer of hybrid nanofluids with thermal

radiation and Joule heating effects. *Case Studies in Thermal Engineering*, 35, 102123.

[16] Sulochana, C., & Ashwinkumar, G. P. (2024). Optimization of electromagnetohydrodynamic nanofluid transport for advanced coating processes. *International Communications in Heat and Mass Transfer*, 151, 107205.